Design, characterisation, and clinical evaluation of a novel porous Ti-6Al-4V hemipelvic prosthesis based on Voronoi diagram

Zhuangzhuang Li[1,2,#], Yi Luo[1,2,#], Minxun Lu[1,2], Yitian Wang[1,2], Linsen Zhong[3], Yong Zhou[1,2], Zhenfeng Duan[4], Li Min[1,2,*], Chongqi Tu[1,2,*]

Key Words:

3D printing; biomimetic prosthesis; bone tumour; pelvic defect reconstruction; porous structure

From the Contents

ABSTRACT

Three-dimensional printed Ti-6Al-4V hemipelvic prosthesis has become a current popular method for pelvic defect reconstruction. This paper presents a novel biomimetic hemipelvic prosthesis design that utilises patient-specific anatomical data in conjunction with the Voronoi diagram algorithm. Unlike traditional design methods that rely on fixed, homogeneous unit cell, the Voronoi diagram enables to create imitation of trabecular structure (ITS). The proposed approach was conducted for six patients. The entire contour of the customised prosthesis matched well with the residual bone. The porosity and pore size of the ITS were evaluated. The distribution of the pore size ranged from 500 to 1400 μm. Porosity calculations indicated the average porosity was 63.13 ± 0.30%. Cubic ITS samples were fabricated for micrograph and mechanical analysis. Scanning electron microscopy images of the ITS samples exhibited rough surface morphology without obvious defects. The Young's modulus and compressive strength were 1.68 ± 0.05 GPa and 174 ± 8 MPa, respectively. Post-operative X-rays confirmed proper matching of the customised prostheses with the bone defect. Tomosynthesis-Shimadzu metal artifact reduction technology images indicated close contact between the implant and host bone, alongside favourable bone density and absence of resorption or osteolysis around the implant. At the last follow-up, the average Musculoskeletal Tumour Society score was 23.2 (range, 21–26). By leveraging additive manufacturing and Voronoi diagram algorithm, customised implants tailored to individual patient anatomy can be fabricated, offering wide distribution of the pore size, reasonable mechanical properties, favourable osseointegration, and satisfactory function.

Introduction

The pelvis is a common site for primary and metastatic bone tumours.[1-3] With the development of neoadjuvant chemotherapy as well as the advances in imaging technology and surgical techniques, limb salvage surgery has become the preferred treatment modality for most patients with pelvic tumours.[4] Nevertheless, tumour resection and pelvic reconstruction remain challenging, especially regarding choosing an appropriate reconstruction method.

Traditionally, orthopaedic surgeons have relied on standard off-the-shelf implants, such as saddle prosthesis,[5, 6] ice cream cone prosthesis,[7, 8] and modular hemipelvic prosthesis.[9-11] While these approaches have yielded favourable outcomes in many cases, they often fall short in reconstructing the intact pelvic ring or transferring the biomechanical load.[12] Moreover, mismatch in elastic modulus and limited osseointegration are the main concerns for the durable fixation of these dense implants.[13]

In recent years, the integration of additive manufacturing (AM) technology (also known as three-dimensional (3D) printing) with biomedical engineering has resulted in groundbreaking advances in orthopaedics.[14] It is possible to fabricate customised implants tailored to the patient-specific anatomical.[15, 16] Therefore, 3D-printed customised hemipelvic prosthesis is hypothesised as an appealing instrument for pelvic defect reconstruction.[3, 15, 17, 18] The anatomically conforming shape and reasonable biomechanical load conduction are believed to help patients obtain favourable clinical outcomes.[19] In addition, AM technologies enable the fabrication of porous Ti-6Al-4V scaffolds with interconnected network, such as electron beam melting (EBM) and selective lase melting. The introduction of porous structures has drastically reduced the elastic modulus of the implant.[20, 21] Meanwhile, the porous structures provide spaces for bone ingrowth, which could improve the osseointegration of the implant.[22] Following these unique features, 3D-printed customised hemipelvic prosthesis with porous structures has become a current popular method for pelvic defect reconstruction.

The pore characteristics of Ti-6Al-4V scaffold have a significant influence on bone ingrowth because of the effects on cell adhesion and nutrient transport.[23, 24] Therefore, porous structure design is one of the focuses of scientists. Several types of porous structure with good mechanical performance have been developed, such as cubic, diamond, face-centred cubic, body-centred cubic, and triply periodic minimal surfaces.[25, 26] Due to their high controllability and certain osteointegration ability, these homogeneous porous structures are also the mainstream choice in clinical application to create porous implants. However, the fixed pore size and shape are quite different from the composition of natural trabecular tissue, which is a highly irregular porous structure.[27] Recently, further studies have proposed that ideal bone tissue engineering scaffolds should simulate the natural bone porous structure.[28, 29] The Voronoi diagram, a promising computational technique, has gained attention due to its ability to create biomimetic structures that closely mimic the natural architecture of bone.[27, 30] Unlike traditional porous designs that typically employ regular, homogeneous pore sizes, the Voronoi diagram enables to create imitation of trabecular structure (ITS). This biomimetic approach has the potential to provide more effective osseointegration and reduce the risk of implant loosening over time. Nevertheless, the study on the biomimetic design and clinical application of customised implants using this technique remains limited. The feasibility and clinical efficacy of this approach is unclear.

This study introduces a novel biomimetically designed hemipelvic prosthesis with ITS by leveraging patient-specific anatomical data and the Voronoi diagram algorithm. Through a series of clinical cases, the feasibility and clinical efficacy of the proposed approach in reconstructing pelvic defects and enhancing patient outcomes were evaluated.

Methods
Subjects
This is a retrospective study after approval by the Ethics Committee of West China Hospital, Sichuan University, and it was performed in accordance with the *Declaration of Helsinki* as revised in 2008. The patients signed the informed consent form before surgery. Six patients who received this biomimetically designed hemipelvic prosthesis for pelvic reconstruction were identified between January 2022 and January 2023. All the patients met the following inclusion criteria: (1) definite pathological diagnosis of primary benign or malignant bone tumour, or solitary metastatic lesion; (2) good response to systemic treatment; and (3) consent for using a 3D-printed customised implant. The exclusion criteria were (1) life expectancy less than 6 months and (2) lesions involving important neurovascular structures. The patient's demographic and clinical characteristics are presented in **Table 1**. Each patient underwent comprehensive imaging assessments of the pelvis, including X-rays, 3D computed tomography (CT), and magnetic resonance imaging.

Table 1. Demographics, clinical characteristics, and follow-up outcomes of six patients

Case	Sex	Age (year)	Diagnosis	Enneking zone	Operation time (minute)	Blood loss (mL)	Follow-up (month)	MSTS score	Complication	Oncological status
1	M	55	Chondrosarcoma	II+III	330	300	24	25	–	NED
2	F	48	Metastasis	II	358	700	22	25	–	AWD
3	F	53	Metastasis	I+II+III	195	400	23	24	–	AWD
4	M	67	Chondrosarcoma	I+II+III	295	1500	18	22	–	NED
5	M	45	Haemangioma	I+II+III	316	3000	20	23	DWH	NED
6	F	61	Metastasis	I+II+IV	314	5000	15	20	–	AWD

Note: MSTS score was obtained at the last follow-up. AWD: alive with disease; DWH: delayed wound healing; F: female; M: male; MSTS: Musculoskeletal Tumour Society; NED: no evidence of disease.

1 Orthopaedic Research Institute and Department of Orthopaedics, West China Hospital, Sichuan University, Chengdu, Sichuan Province, China; 2 Model Worker and Craftsman Talent Innovation Workshop of Sichuan Province, Chengdu, Sichuan Province, China; 3 Tianqi Additive Manufacturing Co., Ltd, Chengdu, Sichuan Province, China; 4 Department of Orthopaedic Surgery, Sarcoma Biology Laboratory, Sylvester Comprehensive Cancer Centre, and The University of Miami Miller School of Medicine, Miami, FL, USA.

Custom prosthesis design and morphological assessment
The hemipelvic prosthesis was designed individually for each patient according to patient-specific anatomical data. Firstly, the CT data (DICOM format) were collected and imported into Mimics software (version 21.0, Materialise, Leuven, Belgium) for segmenting the pelvic 3D model (**Figure 1A**). Then, the osteotomy planes with safe margin were determined based on the combined evaluation of CT and magnetic resonance imaging (**Figure 1B**). Subsequently, simulating osteotomy was performed based on the 3D model (**Figure 1C**). Meanwhile, the guiding plate for bone-cutting was designed, with its internal surface fitting the cortical bone (**Figure 1D**). To formulate the preliminary shape of the prosthesis, the 3D model of the contralateral unaffected hemipelvis was mirrored.

Then, the prosthesis model was modified by smoothing and incorporating specific components, such as screw holes, side-plate, and suture holes (**Figure 1E**).

The ITS was created through the Voronoi diagram algorithm. Firstly, the porous part and solid architecture were strategically engineered in the hemipelvic prosthesis model to optimise mechanical strength and enhance osseointegration (**Figure 1F**). Subsequently, the separated models were imported into 3-Matic software (version 15.0, Materialise). The function block of the "Voronoi Based Lattice" was utilised for porous structure creation (**Figure 1G**). Then, the "target pore radius" and "thickness" were meticulously adjusted to obtain the desired pore size. Finally, the processed models were saved as a print file.
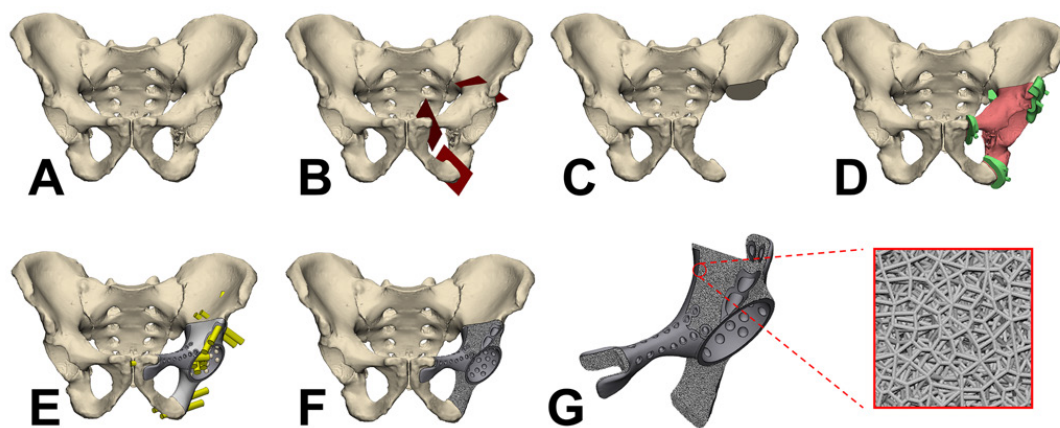

Figure 1. Workflow of designing the customised hemipelvic prosthesis with ITS. (A–G) Segmentation of the pelvis 3D model (A), determination of the osteotomy planes (B), simulation of the tumour resection (C), design of the guiding plate for bone-cutting (D), prosthesis model by mirroring the contralateral unaffected hemipelvis, followed by modifications (E), distribution of the porous part and solid architecture within the prosthesis model (F), creation of the ITS through the Voronoi diagram (G). 3D: three-dimensional; ITS: imitation of trabecular structure.

After the final design was completed, the overall contour of the customised prosthesis was evaluated at the anteroposterior, inlet, and outlet views using the 3-Matic software. Then, the volume of the customised prosthesis was measured using the software, which is based on the enclosed geometry of the 3D model. The porosity was calculated using the following equation:

$$Porosity\,(\%) = (V_0 - V_1)/V_0 \times 100\% \quad (1)$$

where V_0 and V_1 present apparent total volume and porous structure volume, respectively. The pore size was evaluated by the "pore sphere" in the unit cell of the lattice structure, which takes the centroid of the Voronoi unit cell as the sphere centre and the shortest distance to each beam as the radius.

Preparation of printing powder and characterisation of the porous structure
The EBM process (ARCAM Q10plus, Arcam AB, Mölndal, Sweden) was selected for this study due to its ability to

produce high density metal parts with excellent mechanical properties,[31] which are essential for load-bearing implants like the hemipelvic prosthesis. Before printing, Ti-6Al-4V alloy powder (Chunli Co., Ltd., Beijing, China) suitable for EBM process was prepared. The powder was analysed using scanning electron microscopy (SEM) coupled with energy dispersive spectroscopy (Zeiss Sigma 360, Carl Zeiss AG, Oberkochen, Germany). The SEM provided detailed imaging of the powder's surface morphology, while the energy dispersive spectroscopy was used to perform elemental analysis. The particle size was determined using a laser scattering particle size analyzer (Mastersizer, Malvern Panalytical Malvern, UK). In detail, 500 mg of the alloy powder was prepared for the analysis, in accordance with the instrument's specifications. The measurement was carried out using deionised water as the dispersant in a wet testing setup.

Cubic ITS samples of $10 \times 10 \times 10\ mm^3$ were fabricated. The micrograph was examined through SEM (Zeiss) and

micro-CT scanner (VivaCT40, Scanco Medical, Brüttisellen, Switzerland). The compressive experiment was conducted using a computer-controlled electronic universal testing machine (CMT6103, MTS, Eden Prairie, MN, USA). The loading rate was set at 0.1 mm/min. The strain (ϵ) was calculated based on the displacement of the testing machine according to the following the formula:

$$\epsilon\,(\%) = L_1/L_0 \times 100 \qquad (2)$$

where: L_1 is the displacement (the change in length of the sample during compression), L_0 is the original length of the sample before compression (10 mm).

Fabrication of the customised prosthesis and clinical application

All prostheses were manufactured by Chunli Co. After fabrication, the prostheses underwent processing, polishing, and cleaning to ensure they met the required specifications. Additionally, trial models and guiding plates for bone-cutting were fabricated using nylon powder, and resin pelvis models were prepared to help surgical planning and ensure accurate implant placement in surgery.

All the patients underwent surgical treatment in the Department of Orthopaedics, West China Hospital. Under general anesthesia, patients were placed in a lateral position or floating position. Following the separation of surrounding tissues, osteotomy was performed with the assistance of guiding plate for bone-cutting. Subsequently, the accuracy of excision was verified using a nylon trial prosthesis. Upon satisfactory placement, the authentic hemipelvic prosthesis was meticulously inserted into the prepared bone defect, followed by the insertion of screws to secure the prosthesis firmly in position. The constrained acetabular pad was then affixed within the acetabular cup of the prosthesis, and the proximal femoral prosthesis was implanted accordingly. Remaining muscles were sutured to the corresponding parts of the prosthesis through designed suture holes. Subsequently, the incision was sutured in layers, and a drainage tube was inserted to facilitate drainage. Surgical information, including operation duration and estimated blood loss, was diligently recorded for comprehensive assessment of surgical outcomes.

Follow-up and outcome assessment

Patients received monthly follow-up visits for the initial 3 months post-surgery, followed by appointments every 3 months thereafter. At each follow-up visit, a comprehensive assessment was conducted, including radiological and functional evaluations. Specifically, X-rays were employed to monitor the placement, stability, and alignment of the implant. Tomosynthesis-Shimadzu metal artifact reduction technology was utilised to assess the interface between the implant with ITS and the host bone. Functional outcomes were evaluated using the Musculoskeletal Tumour Society 93 score.[32] Additionally, any complications arising during the follow-up period were diligently documented for comprehensive monitoring.

Statistical analysis

Statistical analyses were conducted utilising SPSS statistics software (version 22; IBM Corp., Armonk, NY, USA). Descriptive statistics were used to summarise the patient demographics, clinical characteristics, and follow-up outcomes. These continuous variables are expressed as mean ± standard deviation (SD).

Results

Morphological analysis of the prosthesis

Figure 2A shows 3D models of the reconstructed pelvis at the anteroposterior, inlet, and outlet views. It was observed that the entire contour of the prosthesis matched well with the remaining bone. The superior ramus of the pubis was retained to reconstruct the pelvic ring. The ischial ramus was reconstructed for patients with partial preservation of the ischial ramus. Additionally, the prosthesis shape was modified by reducing the ilium wing and eliminating the posterior iliac spines when the majority of the ilium was invaded.

Figure 2B shows the prosthesis models with delicate-defined solid architecture and porous structure. The weight-bearing arch, superior ramus of the pubis, iliac border, plate, and nail track were designed as solid architecture to assure sufficient strength. With regard to the interface between prosthesis and bone, ITS was adopted in the prosthesis to facilitate bone ingrowth. Additionally, the non-weight-bearing area of the prosthesis used the ITS to reduce weight. In particular, "large pore size" (L)-ITS was used in the detached part of the gluteus medius muscle to facilitate muscle attachment, as shown in the green area of the prosthesis models in cases 3–6. As illustrated in magnified 3D models, the ITS simulated the irregular geometry of human bone tissue. The pore size of the Voronoi unit cell was assessed through "pore spheres" analysis (**Additional Figure 1**). **Figure 2C** presents the distribution of the pore size of ITS, ranging from 500 to 1400 µm. The average pore size and porosity of are presented in **Figure 2D**, and **E**. Additionally, the distribution of the pore size among the L-ITS is provided in **Additional Figure 2**, ranging from 500 to 1900 µm. **Table 2** summarises the detailed pore characteristics of six prosthesis models. The average pore size was 917 ± 2.0 µm and 1260 ± 17 µm for ITS and L-ITS, respectively. Porosity calculations indicated the average porosity was 63.13 ± 0.30% and 64.27 ± 0.25% for ITS and L-ITS, respectively.

Powder characterisation and porous structure

The performance of the powder is crucial in ensuring the success of the AM process and the quality of the final prosthesis. As illustrated in **Figure 3A**, the majority of the Ti-6Al-4V powder exhibited a spherical or near-spherical shape, which is favourable for flowability and packing. The chemical composition of the Ti-6Al-4V powder, as presented in **Figure 3B**, and **C**, includes relatively low concentrations of impurities such as carbon, iron, oxygen, nitrogen, and hydrogen, which are essential for maintaining the desired mechanical properties of the fabricated prosthesis. **Figure 3D** shows the particle size distribution, with a d_{50} (median particle size) value of 58.8 µm, indicating the median particle size of the powder. This particle size is within the optimum range for EBM processes.
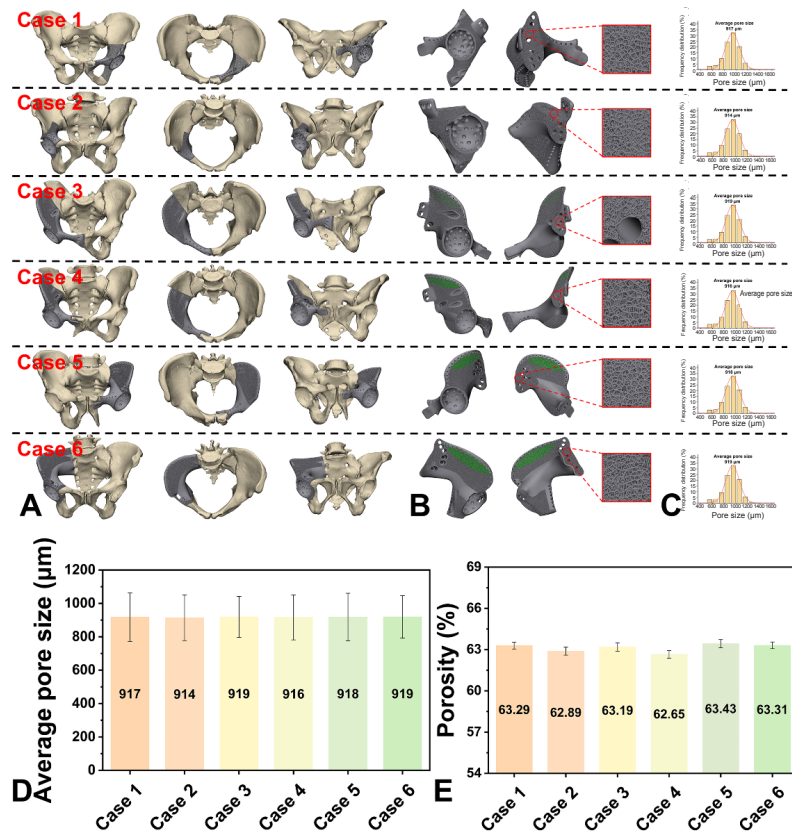
Figure 2. (A) Three-dimensional models of the reconstructed pelvis at the anteroposterior, inlet and outlet views. (B) The prosthesis models with delicate-defined solid architecture and porous structure. (C) The distribution of the pore size ranging from 500 to 1400 μm. (D, E) The average pore size (D) and the porosity (E).

Table 2. Details of the customised hemipelvic prosthesis models

Case	Imitation of trabecular structure				Large pore size-imitation of trabecular structure			
	Distribution of the pore size (μm)	Average pore size (μm)	Unit cell strut thickness (μm)	Porosity (%)	Distribution of the pore size (μm)	Average pore size (μm)	Unit cell strut thickness (μm)	Porosity (%)
1	502–1397	917	400	63.29	–	–	–	–
2	508–1395	914	400	62.89	–	–	–	–
3	501–1398	919	400	63.19	505–1893	1256	600	63.93
4	500–1381	916	400	62.65	509–1897	1285	600	64.54
5	502–1391	918	400	63.43	501–1898	1248	600	64.32
6	503–1390	919	400	63.31	500–1894	1251	600	64.28

The SEM images revealed that both ITS and L-ITS samples exhibit a highly porous architecture that closely mimics the trabecular bone structure (**Figure 4A** and **B**). The pores within these samples are interconnected by disordered struts. The surface morphology of the samples exhibited a rough and irregular texture due to partially melted particles, typical of EBM processes. However, the L-ITS samples demonstrated larger pore sizes, which were strategically designed to facilitate muscle attachment in specific regions of the prosthesis. Micro-CT scans further confirmed the porous network's distribution and the absence of significant defects such as cracks or unmelted holes (**Figure 4C** and **D**). The differences in pore size and porosity between the two samples are evident in these images. Notably, the as-fabricated strut thickness was slightly larger than the intended design, which is attributed to the heat conduction effect that occurs near the electron beam path during the EBM process. The mechanical properties of porous structures were evaluated through the compression test. **Figure 4E** and **F** show the stress-strain curves of the as-fabricated ITS and L-ITS samples, respectively. The elastic modulus of the ITS samples was measured to be 1.68 ± 0.05 GPa. The compressive strength of the ITS samples was determined to be 174 ± 8 MPa. The L-ITS samples presented elastic modulus of 1.38 ± 0.14 GPa and had compressive strength of 115 ± 4 MPa.
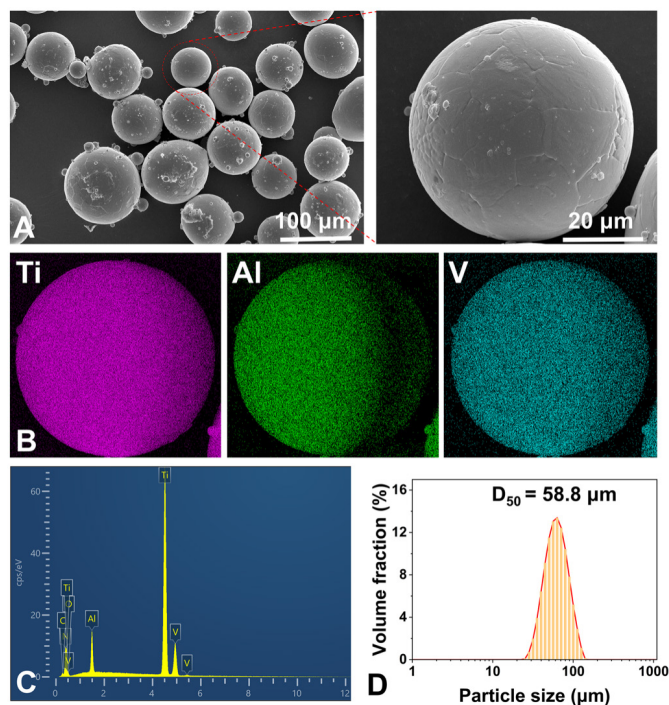
Figure 3. The characterisation of the Ti-6Al-4V powder utilised in this work. (A) Morphology; (B, C) chemical composition; (D) particle size distribution.
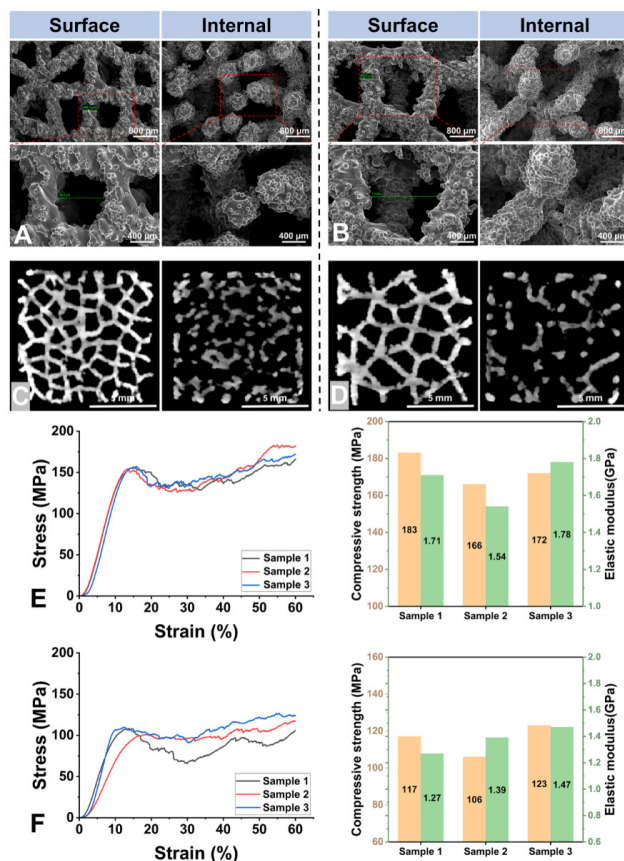

Figure 4. (A, B) SEM images of the cubic ITS and L-ITS samples. (C, D) Micro-CT scans of the cubic ITS and L-ITS samples. (E, F) The stress-strain curves of the as-fabricated ITS and L-ITS samples. ITS: imitation of trabecular structure; L-ITS: large pore size imitation of trabecular structure; Micro-CT: micro-computed tomography; SEM: scanning electron microscopy.

Clinical application and follow-up outcome

Figure 5A displays the prostheses successfully printed by EBM. As depicted, the prostheses were intact without obvious defects. Pre-operatively, surgeons further verified whether the fabricated prosthesis was fitting correctly with the pelvis model. All six patients underwent tumour resection and received prosthesis implantation successfully (**Figure 5B,** and C). The average duration of the operation was 301 minutes (range: 195–358 minutes), with an average blood loss of 1816 mL (range: 300–5000 mL). Intra-operatively, the interface of customised hemipelvic prostheses matched the osteotomy planes. Post-operative pathological examination showed negative surgical margins in all specimens.
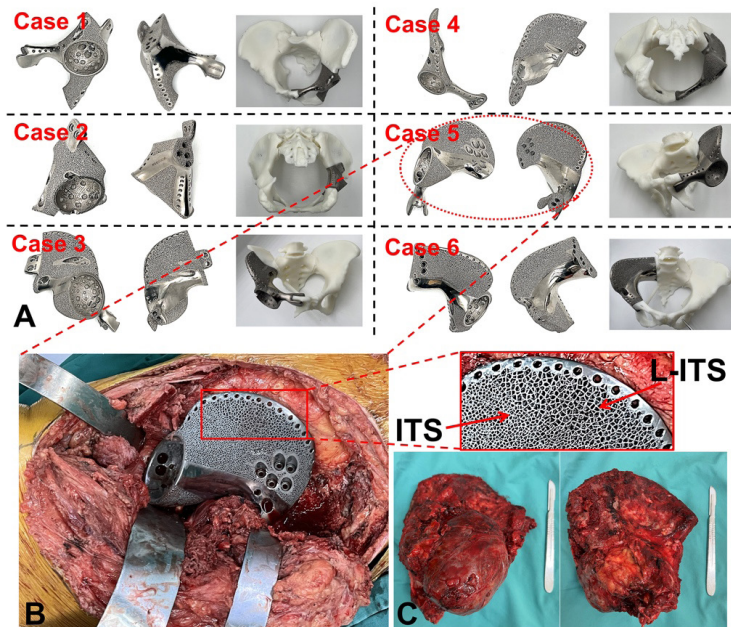

Figure 5. (A) The photographs of prostheses fabricated by EBM. (B, C) Intraoperative photographs of tumour resection and prosthesis implantation. EBM: electron beam melting; ITS: Imitation of trabecular structure; L-ITS: large pore size imitation of trabecular structure.

The average follow-up period was 20.3 months, ranging from 15 to 24 months, with no patients of lost follow-up. Post-operative pelvic X-rays confirmed proper matching of the customised hemipelvic prostheses with the bone defect (**Figure 6**). To quantitatively assess the accuracy of the prosthesis placement, the hip centre of rotation was evaluated by comparing its position vertically and horizontally with the contralateral normal acetabulum. The discrepancy between the prosthetic centre of rotation and the contralateral hip joint was measured. The mean discrepancy of the centre of rotation was 5.1 ± 1.4 mm horizontally and 4.2 ± 0.7 mm vertically, respectively. This small discrepancy indicates a precise alignment of the prosthesis. Tomosynthesis-Shimadzu metal artifact reduction technology images indicated close contact between the implant and host bone, alongside favourable bone density and absence of resorption or osteolysis around the implant. Improved hip function on the prosthetic side was evident, with high patient satisfaction during follow-up assessments. At the last follow-up, the average Musculoskeletal Tumour Society score was 23.2 (range, 20–25). Notably, delayed wound healing occurred in one patient, healing after debridement. No patients of local recurrence or tumour metastasis were observed, and there were no prosthesis-related complications, such as aseptic loosening or structural failure.

Discussion

Pelvic reconstruction following tumour resection presents a significant challenge in orthopaedic surgery because of the complex anatomy and biomechanical demands of the pelvis. Traditional off-the-shelf implants often fail to adequately restore the pelvic ring's integrity although widely used.[12] Additionally, issues such as elastic modulus mismatch and limited osseointegration compromise the long-term fixation.[13] This manuscript introduces a novel approach utilising biomimetic design principle and the Voronoi diagram algorithm to develop hemipelvic prostheses with ITS. The study conducted reconstructions for six individuals with pelvic tumours using this type of customised prosthesis. The results demonstrate promising feasibility and efficacy of the proposed approach in pelvic defect reconstruction.

The customised hemipelvic prostheses can be tailored to each individual's unique anatomy through leveraging AM technology and patient-specific anatomical data. Morphological analysis results in this work revealed that the designed prostheses closely matched the remaining bone. According to Wong et al. study, this biomimetic contour of the prosthesis ensures optimal fit and better biomechanical load distribution, crucial for successful pelvic defect reconstruction.[33] Furthermore,
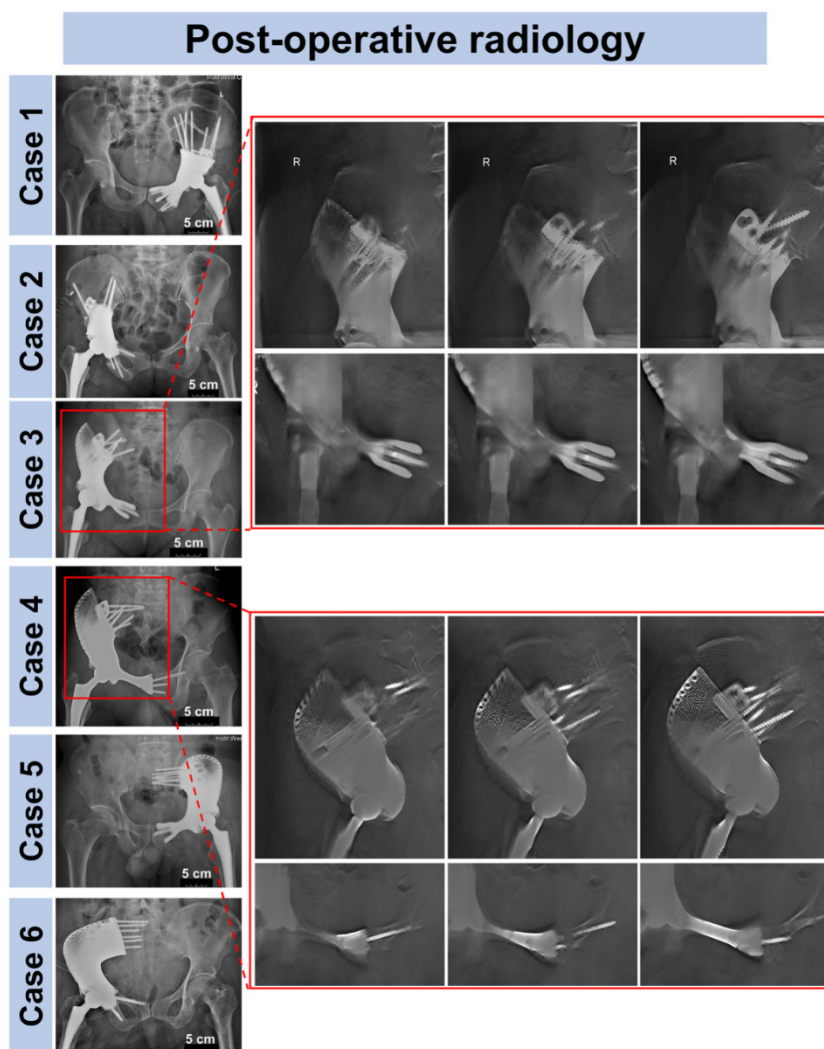
Figure 6. Post-operative pelvic X-rays confirmed proper matching of the customised prostheses with the bone defect. Tomosynthesis-Shimadzu metal artifact reduction technology images of typical 2 patients two months after surgery indicated close contact between the implant and host bone, alongside favourable bone density and absence of resorption or osteolysis around the implant.

porous structures are often incorporated into the prostheses to address elastic modulus mismatch and enhance osseointegration.[34, 35] One of the innovations of this study is the use of the Voronoi diagram algorithm to design the porous structure. Unlike traditional porous structures, which often feature fixed pore sizes and shapes, this algorithm allows for the creation of irregular porous structures.[36-39] Magnifying 3D models illustrated that the created porous structure was closely mimic the natural trabecular architecture of bone tissue. To the best of our knowledge, this is the first study about developing customised hemipelvic prosthesis with such ITS.

It is well known that pore size plays a significant role in osseointegration. However, previous studies have reported very heterogeneous pore size for bone tissue engineering, varying from 20 to 1500 μm.[40, 41] It is generally acknowledged that large pore size is favourable for vascularisation, and greater than 500 μm was recommended.[41] In the past few years, the pore size of porous Ti-6Al-4V used in clinical application

or research has increased to 500–1500 μm.[42] In this work, ITS was designed to have a larger pore size (average of 917 μm) than desired due to the consideration of further decrease of pores size in EBM-fabricated implants. According to "pore spheres" analysis, the wide distribution of the pore size was observed, ranging from 500 to 1400 μm. It is worth noting that in addition to ITS, L-ITS was also designed in the upper area of the prosthesis iliac in cases 3-6. These areas correspond to the detached part of the gluteus medius muscle, and the muscle loss could result in the patient with Trendelenburg gait due to inadequate hip abductor movement.[43] It was reported that large porous would lead to better soft-tissue ingrowth.[44] Therefore, L-ITS with an average pore size of 1260 μm was set to facilitate muscle attachment.

In particular, the micrograph and mechanical properties of the ITS samples were investigated. SEM micrographs presented the absence of significant defects in the as-fabricated ITS samples, indicating good printability and reliability of the

EBM process. It was observed that the introduction of IPS significantly reduced the modulus of solid Ti-6Al-4V. The elastic modulus (< 2 GPa) aligned closely with cancellous bone (0.02 – 2 GPa).[45] Therefore, ITS interface in the customised prosthesis not only had cancellous bone structure conducive to bone ingrowth, but also with similar elastic modulus avoiding stress shielding. With regard to the strength of ITS, the compressive test showed that the ultimate strength of 174 MPa was close to cortical bone. Compared with ITS, the elastic modulus and ultimate strength of L-ITS were further decreased. It is reasonable that the larger pore size contributed to the decrease of elastic modulus and strength under similar porosity (63.13% *versus* 64.27%). Nevertheless, there were many solid architectures in prosthesis to assure sufficient strength, including weight-bearing arch, superior ramus of the pubis, iliac border, plate, and nail track. These results support the feasibility of this biomimetic Ti-6Al-4V hemipelvic prosthesis in pelvic reconstruction.

The clinical application of the customised hemipelvis prostheses in six patients with pelvic tumours yielded promising results.

Actually, the importance of interface osseointegration in ensuring implant stability has been frequently emphasised.[46-48] Especially for the hemipelvic prostheses, simple screw fixation may lead to screw breakage and loosening due to the shear loading on account of the flat interface.[49] In the present study, post-operative radiographic evaluations further confirmed the accurate placement and stability of the implants. Additionally, Tomosynthesis-Shimadzu metal artifact reduction technology images revealed close contact between the implant and host bone interface, indicative of favourable osseointegration without evidence of bone resorption or osteolysis. During the follow-up period, there was no prosthesis-related complications, such as aseptic loosening or structure failure. These results suggest the feasibility and reliability of the customised hemipelvic prostheses with ITS in clinical application. These findings are further supported by the comparison with other studies using different types of 3D-printed implants, as summarised in **Table 3**.[12, 18, 33, 50] The use of the Voronoi diagram algorithm in our design achieved wider distribution of the pore size compared to other designs.

Table 3. Previous studies on the application of three-dimensional-printed hemipelvic prosthesis

Study	Porous type	Pore size (μm)	Mean follow-up (month)	Osseointegration outcome	Mechanical stability outcome	Patient-reported outcomes (MSTS score)
Wong et al.[33]	Regular	720	10	NA	No loosening	NA
Peng et al.[12]	Honeycomb like	400–450	33	NA	No loosening	19.8
Xu et al.[18]	Irregular	600	22	Good	No loosening	22.0
Han et al.[50]	Regular	400	12	NA	No loosening	16.0
Current study	Voronoi-based	917 (500–1400)	20	Good	No loosening	23.2

Note: MSTS: Musculoskeletal Tumour Society; NA: not available.

Several limitations of this study warrant acknowledgment. Firstly, it is imperative to recognise that this study adopted a retrospective design, devoid of a control group. Secondly, the inclusion criteria comprising specific tumour types, alongside variations in patient age and tumour staging at the onset of treatment, might engender incomplete reporting in the study's conclusions. Thirdly, the duration of follow-up was relatively short, compounded by the modest sample size of the present study cohort. Given these constraints, the imperative for larger-scale controlled investigations with prolonged follow-up periods becomes apparent.

By leveraging AM and Voronoi diagram algorithm, customised hemipelvic prosthesis tailored to individual patient anatomy can be fabricated, offering wide distribution of the pore size, reasonable mechanical properties, favourable osseointegration, and satisfactory function. Additionally, future research could explore the application of this technology in other types of bone reconstructions, such as long bone defects, spinal fusions, and complex joint replacements.

Author contributions

Conceptualisation: ZL, ZD and LM; methodology: ZL and LZ; writing—original draft: ZL; data curation, formal analysis, and investigation: YL; visualisation: ML and YW; validation: ML, YW and LZ; writing—review and editing: YZ, ZD, LM and CT; supervision: LM and CT: project administration: CT. All authors read and approved the final version of the manuscript.

Conflicts of interest statement

The authors declare that they have no known competing financial interests or personal relationships that could have appeared to influence the work reported in this paper.

Additional file

Additional Figure 1: The pore size of the Voronoi unit cell was assessed through "pore sphere" analysis.

Additional Figure 2: The distribution of the pore size among the L-ITS ranges from 500 to 1900 μm.

1. Hu, X.; Chen, Y.; Cai, W.; Cheng, M.; Yan, W.; Huang, W. Computer-aided design and 3D printing of hemipelvic endoprosthesis for personalized limb-salvage reconstruction after periacetabular tumor resection. *Bioengineering (Basel).* **2022,** *9,* 400.

2. Du, X.; Wei, H.; Zhang, B.; Gao, S.; Li, Z.; Yao, W. The pedicled sartorius flap and mesh (PSM) technique vs no reconstruction in

repairing the defect after type III pelvic bone tumor resection: a retrospective study. *World J Surg Oncol.* **2023,** *21,* 14.

3. Li, Z.; Lu, M.; Min, L.; Luo, Y.; Tu, C. Treatment of pelvic giant cell tumor by wide resection with patient-specific bone-cutting guide and reconstruction with 3D-printed personalized implant. *J Orthop Surg Res.* **2023,** *18,* 648.

4. Liang, H.; Ji, T.; Zhang, Y.; Wang, Y.; Guo, W. Reconstruction with 3D-printed pelvic endoprostheses after resection of a pelvic tumour. *Bone Joint J.* **2017,** *99-B,* 267-275.

5. Jansen, J. A.; van de Sande, M. A.; Dijkstra, P. D. Poor long-term clinical results of saddle prosthesis after resection of periacetabular tumors. *Clin Orthop Relat Res.* **2013,** *471,* 324-331.

6. Danışman, M.; Mermerkaya, M. U.; Bekmez, Ş.; Ayvaz, M.; Atilla, B.; Tokgözoğlu, A. M. Reconstruction of periacetabular tumours with saddle prosthesis or custom-made prosthesis, functional results and complications. *Hip Int.* **2016,** *26,* e14-18.

7. Issa, S. P.; Biau, D.; Babinet, A.; Dumaine, V.; Le Hanneur, M.; Anract, P. Pelvic reconstructions following peri-acetabular bone tumour resections using a cementless ice-cream cone prosthesis with dual mobility cup. *Int Orthop.* **2018,** *42,* 1987-1997.

8. Fisher, N. E.; Patton, J. T.; Grimer, R. J.; Porter, D.; Jeys, L.; Tillman, R. M.; Abudu, A.; Carter, S. R. Ice-cream cone reconstruction of the pelvis: a new type of pelvic replacement: early results. *J Bone Joint Surg Br.* **2011,** *93,* 684-688.

9. Wang, B.; Xie, X.; Yin, J.; Zou, C.; Wang, J.; Huang, G.; Wang, Y.; Shen, J. Reconstruction with modular hemipelvic endoprosthesis after pelvic tumor resection: a report of 50 consecutive cases. *PLoS One.* **2015,** *10,* e0127263.

10. Guo, W.; Li, D.; Tang, X.; Yang, Y.; Ji, T. Reconstruction with modular hemipelvic prostheses for periacetabular tumor. *Clin Orthop Relat Res.* **2007,** *461,* 180-188.

11. Zang, J.; Guo, W.; Yang, Y.; Xie, L. Reconstruction of the hemipelvis with a modular prosthesis after resection of a primary malignant peri-acetabular tumour involving the sacroiliac joint. *Bone Joint J.* **2014,** *96-B,* 399-405.

12. Peng, W.; Zheng, R.; Wang, H.; Huang, X. Reconstruction of bony defects after tumor resection with 3D-printed anatomically conforming pelvic prostheses through a novel treatment strategy. *Biomed Res Int.* **2020,** *2020,* 8513070.

13. Hu, X.; Lu, M.; Zhang, Y.; Li, Z.; Wang, J.; Wang, Y.; Xing, Z.; Yang, X.; Tu, C.; Min, L. Pelvic-girdle reconstruction with three-dimensional-printed endoprostheses after limb-salvage surgery for pelvic sarcomas: current landscape. *Br J Surg.* **2023,** *110,* 1712-1722.

14. Kelly, C. N.; Evans, N. T.; Irvin, C. W.; Chapman, S. C.; Gall, K.; Safranski, D. L. The effect of surface topography and porosity on the tensile fatigue of 3D printed Ti-6Al-4V fabricated by selective laser melting. *Mater Sci Eng C Mater Biol Appl.* **2019,** *98,* 726-736.

15. Wang, J.; Min, L.; Lu, M.; Zhang, Y.; Wang, Y.; Luo, Y.; Zhou, Y.; Duan, H.; Tu, C. What are the complications of three-dimensionally printed, custom-made, integrative hemipelvic endoprostheses in patients with primary malignancies involving the acetabulum, and what is the function of these patients? *Clin Orthop Relat Res.* **2020,** *478,* 2487-2501.

16. Paxton, N. C.; Nightingale, R. C.; Woodruff, M. A. Capturing patient anatomy for designing and manufacturing personalized prostheses. *Curr Opin Biotechnol.* **2022,** *73,* 282-289.

17. Wang, B.; Hao, Y.; Pu, F.; Jiang, W.; Shao, Z. Computer-aided designed, three dimensional-printed hemipelvic prosthesis for peri-acetabular malignant bone tumour. *Int Orthop.* **2018,** *42,* 687-694.

18. Xu, S.; Guo, Z.; Shen, Q.; Peng, Y.; Li, J.; Li, S.; He, P.; Jiang, Z.; Que, Y.; Cao, K.; Hu, B.; Hu, Y. Reconstruction of tumor-induced pelvic defects with customized, three-dimensional printed prostheses. *Front Oncol.* **2022,** *12,* 935059.

19. Wang, M.; Liu, T.; Xu, C.; Liu, C.; Li, B.; Lian, Q.; Chen, T.; Qiao, S.; Wang, Z. 3D-printed hemipelvic prosthesis combined with a dual mobility bearing in patients with primary malignant neoplasm involving the acetabulum: clinical outcomes and finite element analysis. *BMC Surg.* **2022,** *22,* 357.

20. Parthasarathy, J.; Starly, B.; Raman, S.; Christensen, A. Mechanical evaluation of porous titanium (Ti6Al4V) structures with electron beam melting (EBM). *J Mech Behav Biomed Mater.* **2010,** *3,* 249-259.

21. Aufa, A. N.; Hassan, M. Z.; Ismail, Z. Recent advances in Ti-6Al-4V additively manufactured by selective laser melting for biomedical implants: prospect development. *J Alloys Compd.* **2022,** *896,* 163072.

22. Wang, Z.; Wang, C.; Li, C.; Qin, Y.; Zhong, L.; Chen, B.; Li, Z.; Liu, H.; Chang, F.; Wang, J. Analysis of factors influencing bone ingrowth into three-dimensional printed porous metal scaffolds: A review. *J Alloys Compd.* **2017,** *717,* 271-285.

23. Wang, C.; Xu, D.; Li, S.; Yi, C.; Zhang, X.; He, Y.; Yu, D. Effect of pore size on the physicochemical properties and osteogenesis of Ti6Al4V porous scaffolds with bionic structure. *ACS Omega.* **2020,** *5,* 28684-28692.

24. Van Bael, S.; Chai, Y. C.; Truscello, S.; Moesen, M.; Kerckhofs, G.; Van Oosterwyck, H.; Kruth, J. P.; Schrooten, J. The effect of pore geometry on the in vitro biological behavior of human periosteum-derived cells seeded on selective laser-melted Ti6Al4V bone scaffolds. *Acta Biomater.* **2012,** *8,* 2824-2834.

25. Chen, H.; Han, Q.; Wang, C.; Liu, Y.; Chen, B.; Wang, J. Porous scaffold design for additive manufacturing in orthopedics: a review. *Front Bioeng Biotechnol.* **2020,** *8,* 609.

26. Lv, Y.; Wang, B.; Liu, G.; Tang, Y.; Lu, E.; Xie, K.; Lan, C.; Liu, J.; Qin, Z.; Wang, L. Metal material, properties and design methods of porous biomedical scaffolds for additive manufacturing: a review. *Front Bioeng Biotechnol.* **2021,** *9,* 641130.

27. Gómez, S.; Vlad, M. D.; López, J.; Fernández, E. Design and properties of 3D scaffolds for bone tissue engineering. *Acta Biomater.* **2016,** *42,* 341-350.

28. Chen, H.; Liu, Y.; Wang, C.; Zhang, A.; Chen, B.; Han, Q.; Wang, J. Design and properties of biomimetic irregular scaffolds for bone tissue engineering. *Comput Biol Med.* **2021,** *130,* 104241.

29. Liang, H.; Chao, L.; Xie, D.; Yang, Y.; Shi, J.; Zhang, Y.; Xue, B.; Shen, L.; Tian, Z.; Li, L.; Jiang, Q. Trabecular-like Ti–6Al–4V scaffold for bone repair: a diversified mechanical stimulation environment for bone regeneration. *Compos B Eng.* **2022,** *241,* 110057.

30. Liang, H.; Yang, Y.; Xie, D.; Li, L.; Mao, N.; Wang, C.; Tian, Z.; Jiang, Q.; Shen, L. Trabecular-like Ti-6Al-4V scaffolds for orthopedic: fabrication by selective laser melting and in vitro biocompatibility. *J Mater Sci Technol.* **2019,** *35,* 1284-1297.

31. Zhang, L. C.; Liu, Y.; Li, S.; Hao, Y. Additive manufacturing of titanium alloys by electron beam melting: a review. *Adv Eng Mater.* **2018,** *20,* 1700842.

32. Enneking, W. F.; Dunham, W.; Gebhardt, M. C.; Malawar, M.; Pritchard, D. J. A system for the functional evaluation of reconstructive procedures after surgical treatment of tumors of the musculoskeletal system. *Clin Orthop Relat Res.* **1993,** 241-246.

33. Wong, K. C.; Kumta, S. M.; Geel, N. V.; Demol, J. One-step reconstruction with a 3D-printed, biomechanically evaluated custom implant after complex pelvic tumor resection. *Comput Aided Surg.* **2015,** *20,* 14-23.

34. Wang, J.; Min, L.; Lu, M.; Zhang, Y.; Wang, Y.; Luo, Y.; Zhou, Y.; Duan, H.; Tu, C. Three-dimensional-printed custom-made hemipelvic endoprosthesis for primary malignancies involving acetabulum: the design solution and surgical techniques. *J Orthop Surg Res.* **2019,** *14,* 389.

35. Li, Z.; Luo, Y.; Lu, M.; Wang, Y.; Gong, T.; He, X.; Hu, X.; Long, J.; Zhou, Y.; Min, L.; Tu, C. Biomimetic design and clinical application of Ti-6Al-4V lattice hemipelvis prosthesis for pelvic reconstruction. *J Orthop Surg Res.* **2024,** *19,* 210.

36. Li, J.; Yang, Y.; Sun, Z.; Peng, K.; Liu, K.; Xu, P.; Li, J.; Wei, X.; He, X. Integrated evaluation of biomechanical and biological properties of the biomimetic structural bone scaffold: Biomechanics, simulation analysis, and osteogenesis. *Mater Today Bio.* **2024,** *24,* 100934.

37. Liu, J.; Wang, R.; Gong, X.; Zhu, Y.; Shen, C.; Zhu, Z.; Li, Y.; Li, Z.; Ren, Z.; Chen, X.; Bian, W.; Wang, D.; Yang, X.; Zhang, Y. Ti6Al4V biomimetic scaffolds for bone tissue engineering: Fabrication, biomechanics and osseointegration. *Mater Des.* **2023,** *234,* 112330.

38. Wu, Y.; Wang, Y.; Liu, M.; Shi, D.; Hu, N.; Feng, W. Mechanical properties and in vivo assessment of electron beam melted porous structures for orthopedic applications. *Metals.* **2023,** *13,* 1034.

39. Du, Y.; Liang, H.; Xie, D.; Mao, N.; Zhao, J.; Tian, Z.; Wang, C.; Shen, L. Design and statistical analysis of irregular porous scaffolds for orthopedic reconstruction based on voronoi tessellation and fabricated via selective laser melting (SLM). *Mater Chem Phys.* **2020,** *239,* 121968.

40. Loh, Q. L.; Choong, C. Three-dimensional scaffolds for tissue engineering applications: role of porosity and pore size. *Tissue Eng Part B Rev.* **2013,** *19,* 485-502.

41. Wang, C.; Xu, D.; Lin, L.; Li, S.; Hou, W.; He, Y.; Sheng, L.; Yi, C.; Zhang, X.; Li, H.; Li, Y.; Zhao, W.; Yu, D. Large-pore-size Ti6Al4V scaffolds with different pore structures for vascularized bone regeneration. *Mater Sci Eng C Mater Biol Appl.* **2021,** *131,* 112499.

42. Yin, B.; Ma, P.; Chen, J.; Wang, H.; Wu, G.; Li, B.; Li, Q.; Huang, Z.; Qiu, G.; Wu, Z. Hybrid macro-porous titanium ornamented by degradable 3D Gel/nHA micro-scaffolds for bone tissue regeneration. *Int J Mol Sci.* **2016,** *17,* 575.

43. Huang, G.; Ceccarelli, M.; Huang, Q.; Zhang, W.; Yu, Z.; Chen, X.; Mai, J. Design and feasibility study of a leg-exoskeleton assistive wheelchair robot with tests on gluteus medius muscles. *Sensors (Basel).* **2019,** *19,* 548.

44. Chimutengwende-Gordon, M.; Dowling, R.; Pendegrass, C.; Blunn, G. Determining the porous structure for optimal soft-tissue ingrowth: An in vivo histological study. *PLoS One.* **2018,** *13,* e0206228.

45. Almela, T.; Brook, I. M.; Khoshroo, K.; Rasoulianboroujeni, M.; Fahimipour, F.; Tahriri, M.; Dashtimoghadam, E.; El-Awa, A.; Tayebi, L.; Moharamzadeh, K. Simulation of cortico-cancellous bone structure by 3D printing of bilayer calcium phosphate-based scaffolds. *Bioprinting.* **2017,** *6,* 1-7.

46. Zhang, T.; Wei, Q.; Zhou, H.; Jing, Z.; Liu, X.; Zheng, Y.; Cai, H.; Wei, F.; Jiang, L.; Yu, M.; Cheng, Y.; Fan, D.; Zhou, W.; Lin, X.; Leng, H.; Li, J.; Li, X.; Wang, C.; Tian, Y.; Liu, Z. Three-dimensional-printed individualized porous implants: A new "implant-bone" interface fusion concept for large bone defect treatment. *Bioact Mater.* **2021,** *6,* 3659-3670.

47. Song, P.; Hu, C.; Pei, X.; Sun, J.; Sun, H.; Wu, L.; Jiang, Q.; Fan, H.; Yang, B.; Zhou, C.; Fan, Y.; Zhang, X. Dual modulation of crystallinity and macro-/microstructures of 3D printed porous titanium implants to enhance stability and osseointegration. *J Mater Chem B.* **2019,** *7,* 2865-2877.

48. Shah, F. A.; Thomsen, P.; Palmquist, A. Osseointegration and current interpretations of the bone-implant interface. *Acta Biomater.* **2019,** *84,* 1-15.

49. Guo, Z.; Peng, Y.; Shen, Q.; Li, J.; He, P.; Yuan, P.; Liu, Y.; Que, Y.; Guo, W.; Hu, Y.; Xu, S. Reconstruction with 3D-printed prostheses after type I + II + III internal hemipelvectomy: Finite element analysis and preliminary outcomes. *Front Bioeng Biotechnol.* **2022,** *10,* 1036882.

50. Han, Q.; Zhang, K.; Zhang, Y.; Wang, C.; Yang, K.; Zou, Y.; Chen, B.; Wang, J. Individual resection and reconstruction of pelvic tumor with three-dimensional printed customized hemi-pelvic prosthesis: A case report. *Medicine (Baltimore).* **2019,** *98,* e16658.